Minimally invasive battery-less microcontroller enabled implantable NFC tag for healthcare sensing applications

Paul S. Taylor
Division of Computing, Engineering and Mathematical Sciences, University of Kent
Canterbury, UK, p.taylor-250@kent.ac.uk

John C. Batchelor
Division of Computing, Engineering and Mathematical Sciences, University of Kent
Canterbury, UK, j.c.batchelor@kent.ac.uk

Abstract—**This paper presents a minimally invasive battery-less microcontroller enabled implant that utilizes near-field communication technology to both power and transfer data to and from the implanted device. The implant has been designed around a cylindrical glass vial for its housing, of the type found in pet and livestock identification. Requiring just an injector assembly for implantation it can be deemed as minimally invasive. The prototype tag incorporates a near-field communication front end, providing data transfer and power to a microcontroller and a light emitting diode array, with a maximum measured read range of ~ 5 mm off the skin surface. Although light technology can be used for neural stimulation here it is used as a proof of concept before enabling further sensing modalities. The tag is proposed for use as a wireless platform for patient health monitoring in both clinical and home environments using a smartphone as the reader. It could also have applications in general wellbeing monitoring or sports.**

Keywords—near field communication, NFC, radio frequency identification, RFID, healthcare, monitoring, wellbeing, sports, implant, minimally invasive.

I. INTRODUCTION

An active implantable medical device (AIMD) is a device which relies on an energy source other than that generated by the human body, typically a battery or super capacitor. Common AIMDs are cardiovascular devices [1], glucose monitors [2] – [4], defibrillators [5], neurostimulators [6] cochlear and ocular implants [7] – [9] and micro electro-mechanical systems (MEMS) [10]. A major limitation of these devices is the need for a battery, with a surgical procedure being required to replace exhausted power cells. Inductive charging through the body is possible but has the potential for battery failure, where hazards can include thermal events with the release of heat and electrolyte leakage causing toxic exposure. Also, the battery can potentially be the largest component of an AIMD, possibly limiting placement for space restricted applications. Inductively powering an AIMD offers great potential, even more so if every-day external reading devices incorporating this technology can be utilized rather than application specific hardware.

Beyond simple inventory and asset tracking uses, radio frequency identification (RFID) has great potential in healthcare applications, particularly for wearable and implantable devices. There are several RFID technologies available, used here is near-field communication (NFC), in the high frequency (HF) industrial scientific and medical (ISM) band of 13.56 MHz. When a standard inventory type tag is interrogated by a reader it returns a unique identifier (UID), all wireless and battery free. To enable healthcare sensor applications, in recent years manufacturers have included energy harvesting functionality into some NFC devices [11]. This is where the current induced by the magnetic field generated by the NFC reader is rectified by the device and supplies low-power components such as microcontrollers and associated sensors, with DC powers of up to 15 mW typically available [11]. Being a near field technology NFC range is limited to a few centimetres, and can be platform dependent, but is less affected by the lossy nature of the human body than ultra-high frequency (UHF) RFID.

NFC tags come in a variety of form factors, from credit cards to wearables, fobs and adhesive stickers. These are planar designs that even if made biocompatible would not qualify as suitable for a minimally invasive implant procedure owing to their large area disruption to tissue structure. Another tag type

commonly used for animal tagging are small biocompatible (animal grade) glass cylinders that incorporate a cylindrical ferrite rod inductor. These are available in both NFC and 125 kHz low frequency (LF) technologies. This tag format is suitable for implantation using a syringe implant injector. Pet tags are typically 11 – 13 mm long and 2 mm outer diameter, while larger tags are used in livestock and equine applications. A selection of tag form factors is shown in Fig. 1.

Fig. 1. A selection of planar type NFC tags (1-4). Implantable glass animal tags (5 and 6).

Due to the widespread use of NFC in payment and transport fare systems worldwide, the technology has been included in a majority of currently available smartphones. This makes for a readily available NFC reader where a clinician or end-user can easily interact with an NFC enabled implant to access and store data remotely for further analysis if required.

The proof of concept introduced in this paper features a user programmable LED array that demonstrates functionality through optical feedback, both in terms of energy transfer and communication. Although not regulated for human use the tag is housed in a SCHOTT 8625 animal grade biocompatible glass cylinder [12] as a platform for form fit and function.

II. Development of an Implantable NFC Tag

A. *Communication, Control and Energy Harvesting Electronics*

As well as electrical performance, size constraints are a major factor for minimally invasive implantable tags. The core electronic components required for an NFC AIMD are the NFC device/energy harvester, microcontroller, sensor, display and inductor. The component sizes will dictate the tags housing and final size. A block diagram of the proposed design is shown in Fig. 2.

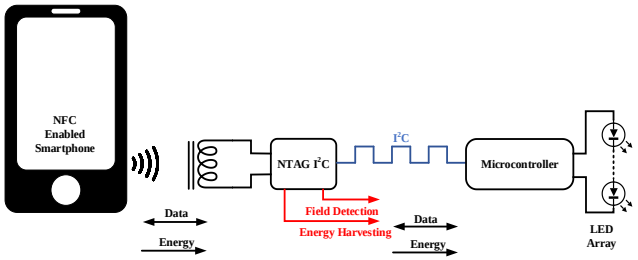

Fig. 2. Proposed design.

The NFC transponder is an NXP NTAG I^2C (NTH3H2211) [13]. This is a fully ISO/IEC 14443A compliant device that includes energy harvesting and 1 or 2K byte EEPROM memory accessible over a serial I^2C bus. Several packages are available with the XQFN8 footprint at $1.6 \times 1.6 \times 0.5$ mm^3 being the smallest and most suitable.

For basic low power sensor applications, high computational requirements are often unnecessary and 8-bit microcontrollers are suitable. The Atmel ATtiny20 [14] selected for this tag is the smallest in its class. The device offers 2K bytes of programmable memory, 10 programmable I/O lines and a 10-bit analog to digital converter in a wafer level chip scale package (WLCSP) of $1.55 \times 1.4 \times 0.54$ mm^3.

B. Reader to Tag Coupling

Although NFC tags – both planar and ferrite rod types – are often referred to as having antennas, being near-field they are actually mutually coupled inductors with operation similar to that of a voltage transformer. For NFC applications inductances in the range of 2 – 3 µH are typical, chosen to resonate with the input capacitance of the NFC device. These values are easily achievable with planar inductors, but for small cylindrical air-core inductances they are not practical. A method of decreasing coil size and achieving the required inductance is to increase its magnetic flux density by inserting a ferrite-core in the windings of the inductor. Ferrite cores come in a range of permeabilities for different frequency applications, with the 67 core series from Fair-Rite [15] being recommended for frequencies > 5.0 MHz and suitable for NFC.

Appropriate alignment between the reader and tag coil is required for successful transfer of energy and data over an NFC link. Although this is straightforward for planar-to-planar cases, such as a contactless card coupling to a point-of-sale reader where the magnetic fields are shown in Fig. 3(a), alignment is more critical for ferrite rod tag coupling to a planar reader coil, Fig. 3(b). In the latter case, the coil should be perpendicular to the tracks of the reader coil. This is due to the magnetic field being axial to the cylindrical tag.

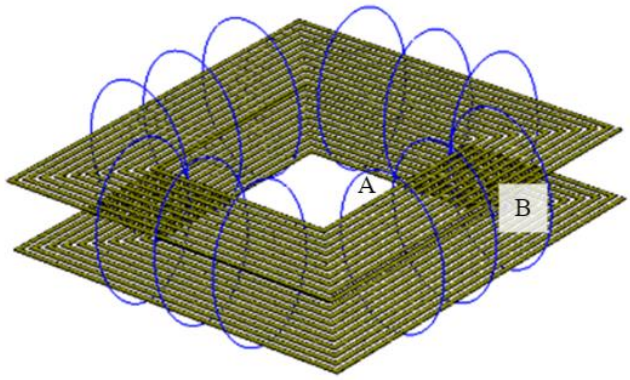

(a)

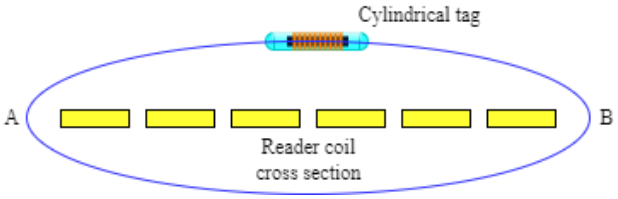

(b)

Fig. 3. Optimal reader/tag coupling alignment where (a) is for the planar case and (b) cross sectional view for a planar reader coil coupling to an implantable ferrite rod type tag. —— Representation of magnetic flux.

III. Design Considerations

Standard NFC tags are typically tuned high in frequency at around 14.5 MHz, but when coupled to a reader at an optimal distance resonance reduces to 13.56 MHz. Although less affected by the human body as the electrical antennas used in UHF RFID, there is still an interaction at HF that needs to be considered in the design, particularly when using high-Q and consequently narrow band devices such as ferrite loaded inductors. To model this effect, using CST MWS™ a tuned circuit representative of the NFC device and inductor tuned to 13.56 MHz was simulated. The inductance is given by (1) where the magnetic former mis 15 mm × 1 mm ferrite rod with a permeability of 67, close wound with 22 turns of 40 s.w.g. enamelled (magnet) copper wire.

$$L = \mu_r \frac{N^2 A}{l} 1.26 \times 10^{-6} \text{ H} \qquad (1)$$

Where:

L is the inductance in henrys.
μ_r is the relative permeability of the core.
N is the number of turns.
A is the are in square meters
l is the length in meters.

The circuit is housed in a SCHOTT 8625 glass vial with the electrical properties, ε_r = 5.6 and loss tangent = 0.007. Using a planar coil for the reader, simulations were carried out to determine resonant frequency and path-loss in-air, and also when implanted at a depth of 2 mm into a homogenous human limb model of ε_r = 21.5 and a loss tangent = 0.6, Fig. 4(a). It is noted from the simulation results in Fig. 4(b) that there is approximately 600 kHz frequency shift in the tag when it is in air as opposed to an implant depth of 2 mm. Allowing for this offset, and that attributed to reader loading, then an in-air tag design of ~ 15 MHz would yield optimum performance when implanted. Path-loss simulations were also carried out for both in-air and 2 mm depth implanted tags, resulting in losses of – 5 and – 10 dB respectively as shown in Fig. 4(c).

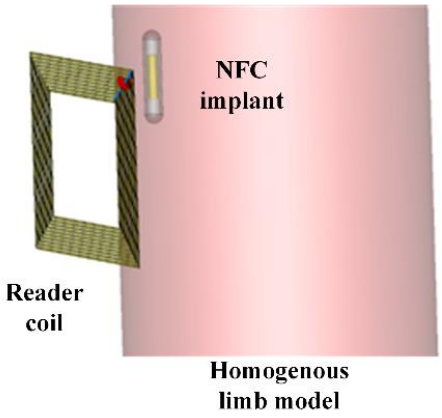

(a)

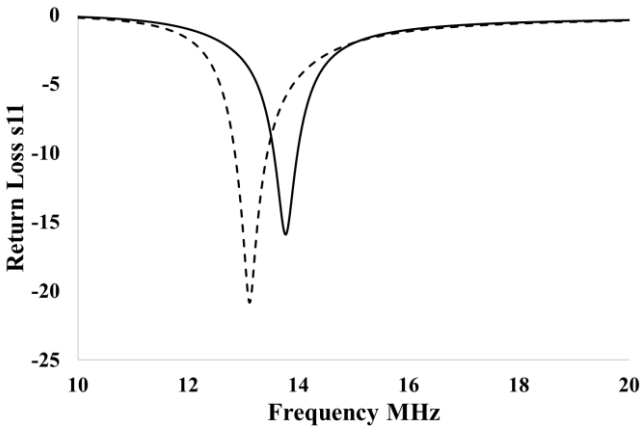

(b)

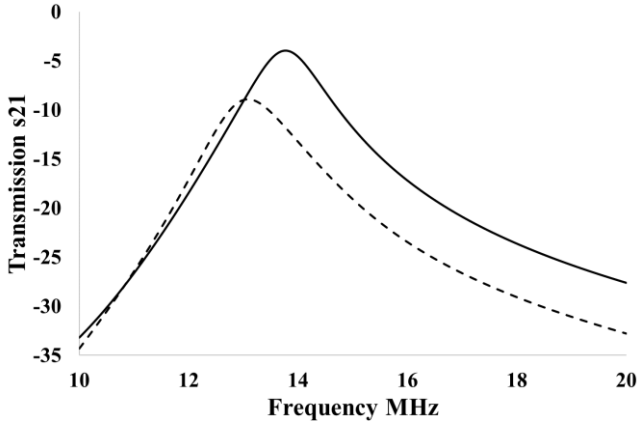

(c)

Fig. 4. (a) CST MWS^{TM} simulation model. (b) Return loss and in (c) path-loss simulations for both in-air ─ and when implanted to a depth of 2 mm ----.

To demonstrate operation, optical feedback is provided by a nine LED array. The microcontroller was programmed with four flash patterns that are selectable over the NFC link using a simple smartphone application. The application NFC Shell [16] allows for reading and writing to specific memory addresses in NFC compliant devices, therefore allowing interaction with the tag. In this case to select different flash patterns.

The combined stack heights of the components and PCB could be accommodated within a 3 mm o.d. 2.49 mm i.d. SCHOTT glass vial, leaving a space of ~ 1.2 mm for the ferrite rod inductor. The selected PCB material was polyimide with a thickness of 0.2 mm. Allowing for tracking and component placement this results in a PCB size of 15 mm × 2.2 mm. The selected glass vial length was 17 mm as this needs to be longer than the PCB to allow for sealing without damaging the PCB and its components. Fig. 5 shows the general construction of the tag.

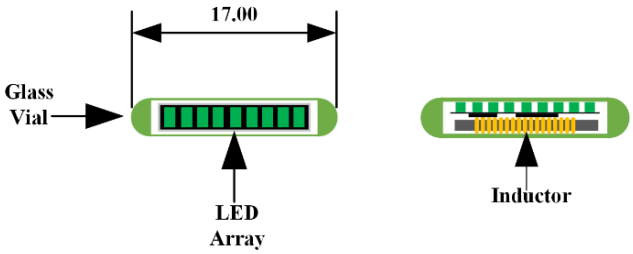

(a) (b)

Fig. 5 (a) Top view of the tag, (b) side view.

IV. Tag Coding and Construction

The ATtiny20 microcontroller does not include a specific I^2C port or the associated registers normally required to communicate with the NTAG NTH3H2211 device. However, this was overcome by emulating the port operation in software. The microcontroller clock was 1 MHz with an I^2C speed of 400 kHz. The code was written in both C and assembler. The test tag was hand assembled, Fig. 6 (a) shows the top and rear of the populated PCB. Of note are the five additional connection pads that are removed after programming the microcontroller. Green LEDs are chosen for maximum light transmission through the green SCHOTT glass.

The two main techniques for sealing glass vials are flame and infrared (IR) laser, with the SCHOTT glass being absorptive at IR frequencies. Here we used the flame sealing technique, where the open-ended vial was heat-sunk in a rotating fixture of ~ 100 rpm and a flame of ~ 1000^{o}C was applied at a 45^o angle to the vial. After a few seconds of applied heat, the glass collapses in upon itself creating a seal as shown in Fig. 6 (b).

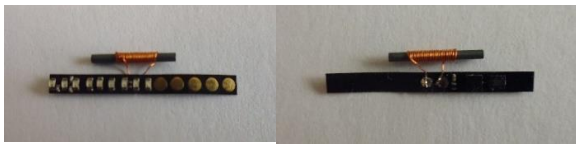

(a)

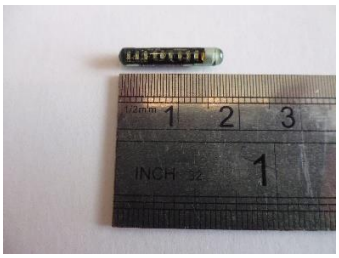

(b)

Fig. 6. (a) Top and rear views of a populated PCB. Top view clearly showing the 9 LED array and the 5 sacrificial programming connections. (b) Tag housed and sealed in SCHOTT 8625 glass.

V. Practical Measurements

A section of pork meat complete with skin and fat was used to emulate an implanted tag. Using a Vector Network Analyzer (VNA) and link coupling to the tag with a pick-up coil, resonant frequency measurements were taken for the tag in air, implanted to a depth of ~ 2 mm, and when coupled to a smartphone reader. The results were ~ 15, 14.2 and 13.6 MHz respectively. An animal injector was used to perform the implantation as shown in Fig. 7(a). Using a Samsung A3 smartphone while coupling perpendicular to the tag the default LED flash pattern is displayed as shown in Fig. 7(b). It should be noted this is a scrolling pattern where only one LED is illuminated at a time.

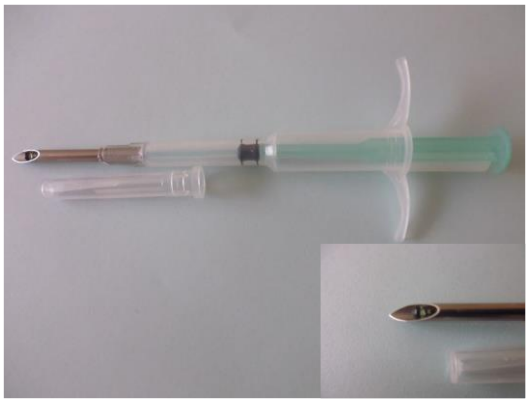

(a)

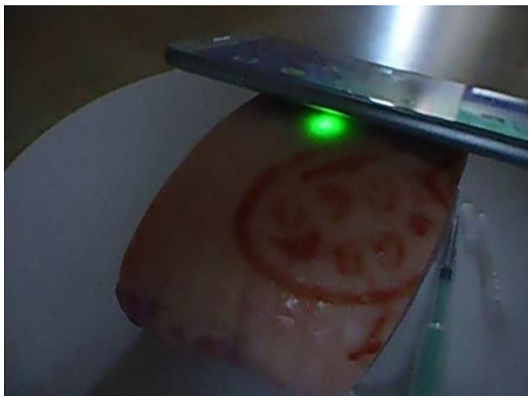

(b)

Fig. 7. (a) Animal injector loaded with the experimental tag. (b) Demonstration of experimental tag injected under the pork skin and coupled over NFC to a smartphone.

Using the programming environment NFC Shell, the byte that controls the flash patterns was incremented, causing the second flash pattern to be displayed. This worked for all additional patterns with the tag defaulting to the first pattern should an incorrect value be entered. Fig. 8 shows a screenshot taken from NFC Shell just after programming a new pattern value. The returned hex value of 0A confirms correct programming of the tag. If an error occurs when programming then the software returns a NAK (negative acknowledgment). This can be attributed to poor coupling between the tag and smartphone due to coil misalignment. The read range was measured to be a maximum of ~ 5 mm off the skin surface.

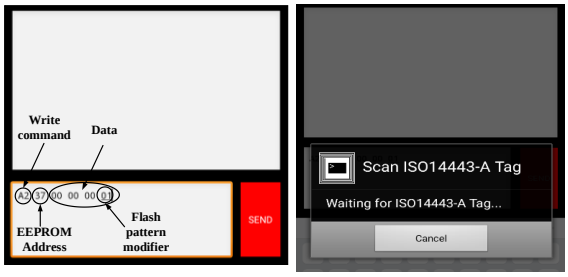

(a) (b)

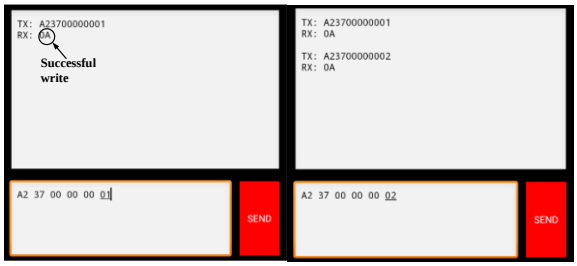

(c) (d)

Fig. 8. Screen shots of NFC Shell in use, where (a) shows the command, address and data to be sent. In (b) the screen presented before coupling to a tag. (c) shows a successful write of flash pattern 01 to the tag and (d) similarly shows the same for pattern 02.

VI. Conclucions

This paper has demonstrated a wireless and battery free, minimally invasive implant with potential for healthcare sensor applications that can be powered and interrogated using an NFC enabled smartphone. The prototype miniaturized tag

and associated electronics are housed in a glass vial of 17 mm × 3 mm making it suitable for insertion using a standard implant type injector. After injecting the tag into a section of pork meat at a depth of ~ 2 mm its electrical performance was tested. Using a standard smartphone and coupling to the tag, the selected flashing LED pattern could be easily observed through the pork skin. Communicating with the tag using the smartphone application NFC Shell, several LED flashing patterns were selected, and each was visually confirmed to be correct through the pig skin. This demonstrates correct operation of the tag in terms of RF energy harvesting and data transfer. A main feature of this approach is that no application specific components or hardware is required with every component and reader being readily available. Future work will incorporate further sensor electronics based upon the platform detailed here for implant applications.

Acknowledgment

This work was supported by UK Engineering and Physical Sciences Research Council EPSRC with grant EP/P027075/1

References

[1] Costa PD, Rodrigues PP, Reis AH, Costa-Pereira A. A review on remote monitoring technology applied to implantable electronic cardiovascular devices. Telemed J E Health. 2010 Dec;16(10):1042-50. doi: 10.1089/tmj.2010.0082. Epub 2010 Nov 11. PMID: 21070132.

[2] B. D. McKean and D. A. Gough, "A telemetry-instrumentation system for chronically implanted glucose and oxygen sensors," in *IEEE Transactions on Biomedical Engineering*, vol. 35, no. 7, pp. 526-532, July 1988, doi: 10.1109/10.4581.

[3] Anabtawi N, Freeman S, Ferzli R. A Fully Implantable, NFC Enabled, Continuous Interstitial Glucose Monitor. IEEE EMBS Int Conf Biomed Health Inform. 2016 Feb;2016:612-615. doi: 10.1109/BHI.2016.7455973. Epub 2016 Apr 21. PMID: 28702512; PMCID: PMC5502769.

[4] A. DeHennis, S. Getzlaff, D. Grice and M. Mailand, "An NFC-Enabled CMOS IC for a Wireless Fully Implantable Glucose Sensor," in *IEEE Journal of Biomedical and Health Informatics*, vol. 20, no. 1, pp. 18-28, Jan. 2016, doi: 10.1109/JBHI.2015.2475236.

[5] K. K. Mahesh and P. Sudheesh, "Design Anaysis of Defibrillator and Implementing Wireless Charging System," *2020 5th International Conference on Communication and Electronics Systems (ICCES)*, 2020, pp. 295-299, doi: 10.1109/ICCES48766.2020.9138026.

[6] H. Lyu, J. Wang, J. La, J. M. Chung and A. Babakhani, "An Energy-Efficient Wirelessly Powered Millimeter-Scale Neurostimulator Implant Based on Systematic Codesign of an Inductive Loop Antenna and a Custom Rectifier," in *IEEE Transactions on Biomedical Circuits and Systems*, vol. 12, no. 5, pp. 1131-1143, Oct. 2018, doi: 10.1109/TBCAS.2018.2852680.

[7] S. Hong, S. Jeong, S. Lee, B. Sim, H. Kim and J. Kim, "Low EMF Design of Cochlear Implant Wireless Power Transfer System using A Shielding Coil," *2020 IEEE International Symposium on Electromagnetic Compatibility & Signal/Power Integrity (EMCSI)*, 2020, pp. 623-625, doi: 10.1109/EMCSI38923.2020.9191460.

[8] M. Ghorbel, A. B. Hamida and J. Tomas, "CMOS RF powering system for cochlear implant," *2009 3rd International Conference on Signals, Circuits and Systems (SCS)*, 2009, pp. 1-4, doi: 10.1109/ICSCS.2009.5412266.

[9] G. D. Chitnis, T. Maleki, B. Samuels, L. B. Cantor and B. Ziaie, "An ocular tack for minimally invasive continuous wireless monitoring of intraocular pressure," 2012 IEEE 25th International Conference on

Micro Electro Mechanical Systems (MEMS), 2012, pp. 922-925, doi: 10.1109/MEMSYS.2012.6170336.

[10] Bazaka, Kateryna, and Mohan V. Jacob. 2013. "Implantable Devices: Issues and Challenges" *Electronics* 2, no. 1: 1-34. https://doi.org/10.3390/electronics2010001

[11] NTAG I²C | Energy harvesting NFC Forum Thttps://www.nxp.com/products/no-longer-manufactured/ntag-ic-energy-harvesting-nfc-forum-type-2-tag:NT3H1101_NT3H1201ype 2 Tag | NXP Semiconductors; Accessed 01/02/2023

[12] https://www.schott.com/en-gb/products/vivotag-p1000295 Accessed 01/02/2023

[13] www.nxp.com/docs/en/data-sheet/NT3H2111_2211.pdf Accessed 01/02/2023

[14] ww1.microchip.com/downloads/en/devicedoc/atmel-8235-8-bit-avr-microcontroller-attiny20_datasheet.pdf Accessed 01/02/2023

[15] www.fair-rite.com/67-material-data-sheet/ Accessed 01/02/2023

[16] https://play.google.com/store/apps/details?id=com.emutag.nfc Shell&hl=en_GB&gl=US Accessed 01/02/2023